Electronic density of state in valence fluctuating kondo lattice systems studied by point-contact spectroscopy (Review article)

Shiga, Masanobu
Department of Applied Quantum Physics, Kyushu University

Maruyama, Isao
Department of Information and Systems Engineering, Fukuoka Institute of Technology

Mitsuda, Akihiro
Department of Physics, Kyushu University

Wada, Hirofumi
Department of Physics, Kyushu University

他

出版情報：Low temperature physics. 49 (7), pp.876-885, 2023-07-01. AIP Publishing
バージョン：

Low Temperature Physics/Fizyka Nyzkykh Temperatur, 2023, Vol. 49, No. 7, pp. 960–971

Electronic density of state in valence fluctuating Kondo lattice systems studied by point-contact spectroscopy

(Review Article)

Masanobu Shiga[1], Isao Maruyama[2], Akihiro Mitsuda[3], Hirofumi Wada[3], and Tatsuya Kawae[1]

[1]*Department of Applied Quantum Physics, Kyushu University, Motooka, Fukuoka 819-0395, Japan*

[2]*Department of Information and Systems Engineering, Fukuoka Institute of Technology, Fukuoka 811-0295, Japan*

[3]*Department of Physics, Kyushu University, Motooka, Fukuoka 819-0395, Japan*

E-mail: shiga.masanobu.881@m.kyushu-u.ac.jp
t.kawae.122@m.kyushu-u.ac.jp

Received February 3, 2023, published online May 26, 2023

This article reviews our recent point-contact spectroscopy (PCS) investigation in valence fluctuating Kondo lattice systems, $EuNi_2P_2$ and Ge-substituted $EuNi_2(P_{0.8}Ge_{0.2})_2$, and YbPd. A heavy fermion (HF) compound $EuNi_2P_2$ exhibits a significant valence fluctuation owing to the intermediate Eu valence of 2.5+ at low temperatures, leading to a strong hybridization between the conduction and *f* electrons (*c*–*f* hybridization). The electronic density of state measurements on $EuNi_2P_2$ by using PCS technique reveal that the HF behavior arises from the formation of the indirect hybridization gap with a double-peak structure near the Fermi level due to *c*–*f* hybridization. In $EuNi_2(P_{0.8}Ge_{0.2})_2$, the valence fluctuation is suppressed by the Ge substitution, and the separation of the double-peak structure decreases. These suggest that the HF behavior is induced by the valence fluctuation. In YbPd, where two-dimensional (2D) layers of Yb^{3+} and $Yb^{2.6+}$ are alternately aligned, a HF-like behavior with a large Sommerfeld coefficient appears at low temperatures in the specific heat. The PCS spectra represent a zero-bias dip structure with an asymmetric background, reproduced by the summation of two Fano curves with two different characteristic temperatures, meaning the formation of two Kondo resonance states for each Yb^{3+} and $Yb^{2.6+}$ site. These suggest that a local coherence causes the large Sommerfeld coefficient in the 2D layers of Yb^{3+}, which are screened by the conduction electrons provided by the valence fluctuating $Yb^{2.6+}$ sites. The observed results indicate that PCS is a powerful technique for examining the variation of electronic DOS in valence fluctuating Kondo lattice systems.

Keywords: point-contact spectroscopy, electronic density of state, Kondo lattice, heavy fermion, valence fluctuation.

1. Introduction

Rare earth compounds with Ce, Eu, and Yb exhibit fascinating phenomena, such as the Kondo effect, heavy fermion (HF) behavior, valence fluctuation, unconventional superconductivity, and non-Fermi liquid behavior [1–3]. In these phenomena, hybridization between the conduction and *f* electrons (*c*–*f* hybridization) plays a key role. According to theory [4, 5], in a Kondo lattice system, in which localized *f* electron moments are periodically arranged, the electronic density of states (DOS) near the Fermi level changes significantly as the temperature decreases below the Kondo temperature T_K. A sharp peak structure, referred to as Kondo resonance, is formed in the electronic DOS at the Fermi level owing to *c*–*f* hybridization. When the temperature is considerably below T_K, the Kondo resonance splits into two peaks owing to an indirect hybridization gap in the DOS [4, 5], in which the gap separation is smaller than the direct gap. Hence, the evolution of the indirect hybridization gap can be examined through an electronic DOS investigation near the Fermi level, which leads to a deeper understanding of the novel phenomena occurring in Kondo lattice systems.

The electronic DOS investigation in Kondo system was performed firstly for single-magnetic impurity on a paramagnetic metal, such as Co atom on Au (111) surface, using

a scanning tunneling spectroscopy (STS) technique. The Kondo resonance has been confirmed through the observation of the Fano resonance [6], which originates from interference between the two tunneling electron paths emitted from a probe tip to the continuous conduction band and localized level arising from the Kondo resonance. The STS technique was also employed to examine the indirect hybridization gap in Kondo lattice systems [7–10]. According to the theoretical study, the indirect hybridization gap is predicted to be detected as an asymmetric double peak structure in the STS spectrum [11]. However, the double peak structure in the Kondo lattice systems has not been observed clearly in the STS spectra, which is likely caused by the low tunneling probability of electrons emitted from a probe tip to the localized *f* orbital. The results indicate that another technique with a high tunneling probability into the localized *f* orbital is indispensable for detecting the indirect hybridization gap.

For this purpose, particular attention has been paid recently to a point-contact spectroscopy (PCS) technique, in which the differential conductance (dI/dV) is measured at a junction formed between a probe tip and sample surface. When the contact size d at the junction is smaller than the electron mean free path l ($d \lesssim l$), the bias voltage dependence of dI/dV spectrum reflects the electronic DOS [12, 13]. Indeed, the PCS technique has been applied for evaluating the electronic DOS in various materials with high-energy resolutions [12–16]. It is significant that in PCS measurements a probe tip touches a sample surface, which gives an essential difference between the PCS and STS investigation, because the latter keeps a gap between the probe tip and sample surface during the measurements. In the investigation of Kondo lattice systems, therefore, the tunneling probability of electrons from a probe tip to the localized *f* orbital in the PCS spectrum is much larger than that in the STS spectrum. The difference between the two measurements is confirmed in the spectra on URu_2Si_2 [17]. The PCS spectra represent an asymmetric double peak structure, which is understood as the emergence of the indirect hybridization gap in the electronic DOS predicted by the theory. In contrast, the double-peak structure is invisible in the STS spectra [7]. These imply that the PCS is useful to examine the evolution of electronic DOS owing to *c–f* hybridization in Kondo lattice systems.

The PCS investigation has been performed in a variety of Kondo lattice systems [12, 17–25]. Moser *et al*., performed PCS investigation on $CeAl_3$, $CeCu_6$, and U-based compounds [18], which show an asymmetric dip structure at around zero bias in differential resistance dV/dI. They considered that the PCS spectra reflect the electronic DOS. In contrast, Naidyuk *et al*., and Paulus and Voss ascribed these spectra to heating effect at the point contact [19, 20]. In Kondo lattice systems, the electron mean free path is decreased by the formation of heavy-fermion state at low temperature. As a result, the transport property in the contact is in the thermal regime ($l < d$), where the bias voltage dependence of PCS spectrum is similar to the temperature dependence of electrical resistivity due to Joule heating at around the contact. Indeed, many PCS spectra in Kondo lattice systems could be explained by considering that the spectra are measured in the thermal regime [12, 21, 22].

Recently, it is revealed that the electronic DOS of Kondo lattice systems can be measured by using PCS technique [17, 23–25]. For instance, PCS spectra for U-based compounds, such as URu_2Si_2 and UPd_2Al_3, exhibit an asymmetric double peak structure arising from the indirect hybridization gap, meaning that the measurements in the ballistic or diffusive regime ($d \lesssim l$) are possible [12, 17, 24]. Nevertheless, the spectra for Ce-based HF compounds, such as $CeCoIn_5$, Ce_3PdIn_{11}, and Ce_2PdIn_8, show an asymmetric dip or peak structure reproduced by the Fano resonance [23, 25], indicating the invisibility of the indirect hybridization gap. Generally, the magnitude of the *c–f* hybridization in Ce-based compounds is smaller than that in U-based compounds, which suggests that the magnitude plays an important role for observing the asymmetric double peak structure due to the indirect hybridization gap. Hence, we focus on the valence fluctuating Kondo lattice systems with a strong *c–f* hybridization to reveal the relation between the spectrum shape and *c–f* hybridization.

In this review, we present our recent PCS investigations on valence-fluctuating Kondo lattice systems, $EuNi_2P_2$ and its Ge-substituted $EuNi_2(P_{0.8}Ge_{0.2})_2$ [26, 27], and YbPd [28, 29]. In $EuNi_2P_2$, the valence value of the Eu ion is ~2.5+ at low temperatures, resulting in strong *c–f* hybridization arising from significant valence fluctuations. The PCS spectra with an asymmetric double-peak structure at approximately zero bias voltage are well-reproduced by the theoretical model proposed by Maltseva *et al*. [11], demonstrating the emergence of an indirect hybridization gap. In $EuNi_2(Ge_{0.2}P_{0.8})_2$, in which the valence fluctuation is suppressed by Ge substitution, the indirect hybridization gap decreases. These results suggest that the origin of the HF state in $EuNi_2P_2$ and $EuNi_2(Ge_{0.2}P_{0.8})_2$ is caused by valence fluctuations and not by spin fluctuations. In YbPd, two Yb layers with valences of 3+ and 2.6+ are alternately aligned at low temperatures, exhibiting a large Sommerfeld coefficient for the specific heat. The PCS spectra show a zero-bias dip structure with an asymmetric background, which can be reproduced by the summation of two Fano curves at different Kondo temperatures. The large Sommerfeld coefficient can be explained by the Kondo effect at the Yb^{3+} sites screened by the conduction electrons provided from the valence-fluctuating $Yb^{2.6+}$ sites.

2. Experimental

Single-crystals of $EuNi_2P_2$, $EuNi_2(P_{0.8}Ge_{0.2})_2$, and YbPd were grown by the Sn-flux [30, 31] and Yb self-flux methods [32], respectively. The sample was placed in a cryostat immediately after the mechanical polishing of its surface.

A homemade PCS apparatus mounted in the cryostat comprised two types of piezo-devices: an attocube piezo-based positioner (ANPz51 attocube systems AG) and a stacked piezo-device. Using these devices, we can change the point-contact size from atomic size to dozens of nanometers [33]. The contact size was maintained constant by controlling the stacked-type piezo-device with a feedback loop during the temperature variation, which enabled the tracking of the PCS spectra over a wide temperature range. A tungsten (W) or platinum (Pt) wire with the diameter of 0.2 mm was used as the probe tip. Differential conductance dI/dV spectra were measured using the lock-in technique.

3. Experimental results

3.1. $EuNi_2(P_{1-x}Ge_x)_2$

In the case of $x = 0$, $EuNi_2P_2$ is a valence fluctuating system with a $ThCr_2Si_2$-type structure. The average Eu valence of $EuNi_2P_2$ monotonically increases from ~ 2.2 + to ~ 2.5+ with decreasing temperature, whereas most intermediate-valence Eu systems show a first-order valence transition at finite temperatures [3, 34]. Hence, the *c–f* hybridization arising from the valence fluctuation in $EuNi_2P_2$ is larger than in other Eu systems at low temperatures. $EuNi_2P_2$ exhibits typical HF behavior owing to strong *c–f* hybridization, as described below. The electronic specific heat coefficient of $EuNi_2P_2$ is ~ 100 mJ/(K^2·mol) [35, 36], indicating that the HF state is formed at low temperatures. As the temperature decreases, the electrical resistivity $\rho(T)$ decreases monotonically after a local maximum at approximately 100 K, exhibiting Fermi liquid behavior with a T^2-dependence below 10 K [36], which is similar to that of Ce- and Yb-based HF systems. The Kondo temperature T_K was estimated to be approximately 80 K based on specific heat and thermal expansion measurements [36]. These results indicate that strong valence fluctuations and HF behavior coexist at low temperatures in $EuNi_2P_2$.

In contrast, in the case of $x = 1$, $EuNi_2Ge_2$ with a stable divalent Eu state shows an antiferromagnetic order at $T_N \approx$ ≈ 30 K. Therefore, the valence value of the Eu ion with 2.5 + is expected to be lowered by Ge substitution for P in $EuNi_2P_2$ owing to the decrease in *c–f* hybridization, resulting in the suppression of the valence fluctuation. Paramanik *et al*. grew $EuNi_2(P_{1-x}Ge_x)_2$ single crystals and revealed that an increase in the Ge concentration causes a gradual change in the ground state from a paramagnetic HF state to an antiferromagnetic ordered state, suggesting that the valence fluctuation gradually decreases with increasing Ge concentration [31]. To reveal the role of valence fluctuation in the emergence of HF behavior in $EuNi_2P_2$ from the viewpoint of the electronic DOS, we performed a PCS investigation on $EuNi_2P_2$ ($x = 0$) and $EuNi_2(P_{0.8}Ge_{0.2})_2$ ($x = 0.2$).

First, we present PCS results for $EuNi_2P_2$. Figure 1(a) shows the dI/dV spectra of the $EuNi_2P_2$/W interface at $T = 5.3$ K. The spectrum exhibits an asymmetric double-peak structure at approximately ± 15 mV. A similar shape appeared in the spectrum when Pt is used as the probe tip, as illustrated in Fig. 1(b), indicating that the asymmetric double-peak structure is an essential feature in the PCS spectra of $EuNi_2P_2$ probed by a normal metal tip.

We checked the local heating effect of the contact owing to the measurements. It is well-known that PCS spectra possess spectroscopic information when the electron scattering is in the ballistic or diffusive regime [12, 13]. In contrast, in the thermal regime, a voltage drop occurs in the vicinity of the point contact owing to the inelastic scattering of the conduction electrons accelerated by the bias voltage, thus resulting in a temperature increase in the vicinity of the point contact. Consequently, the local temperature at the junction T_J is higher than the bath temperature T_{bath} owing to Joule heating [12, 19, 20]. In this case, T_J can be estimated using the following equation:

$$T_J^2 = T_{\text{bath}}^2 + \frac{V^2}{4L}, \qquad (1)$$

where V and L are the applied bias voltage and the Lorenz number, respectively. This equation shows that T_J is increased by applying a bias voltage during the PCS measurements. Additionally, in the thermal regime, the bias voltage dependence of the symmetric component of differential resistance $dV/dI(V)$ is similar to the temperature dependence of the electrical resistivity $\rho(T)$, as observed in the previous PCS investigation on Ce-based HF compounds [12, 21, 22]. We compared the dV/dI curve with the temperature dependence of $\rho(T)$, as shown in Fig. 1(c), which was calculated from the dI/dV spectrum depicted in Fig. 1(a). $\rho(T)$ decreases monotonically after a local maximum at approximately 100 K, whereas the dV/dI shows an upturn below approximately 15 mV. The two curves were different, implying that the local heating effect did not affect the experimental results. From this analysis, we concluded that the measurements were performed in the ballistic or diffusive regime.

The structural disorder at the point contact causes a zero-bias anomaly in the PCS spectra [12, 37, 38]. If the zero-bias anomaly originates from structural disorder, the dip structure should be changed as the point-contact size varies [38]. This means that structural disorder can be excluded as the origin of the double-peak structure by the contact resistance (contact size) dependence of the dI/dV spectra. Figure 1(d) shows the contact-resistance dependence of dI/dV spectra obtained at $T = 4.3$ K. The spectra were measured by increasing the contact resistance from 12 to 60 Ω, which corresponded to a decrease in the contact size. Using the stacked-type piezo-device, PCS spectra were recorded by decreasing the contact size without breaking the point contact. The position of the double-peak structure is independent of the contact size, demonstrating that the asymmetric double-peak structure is not caused by structural disorder but by the electronic DOS in $EuNi_2P_2$.

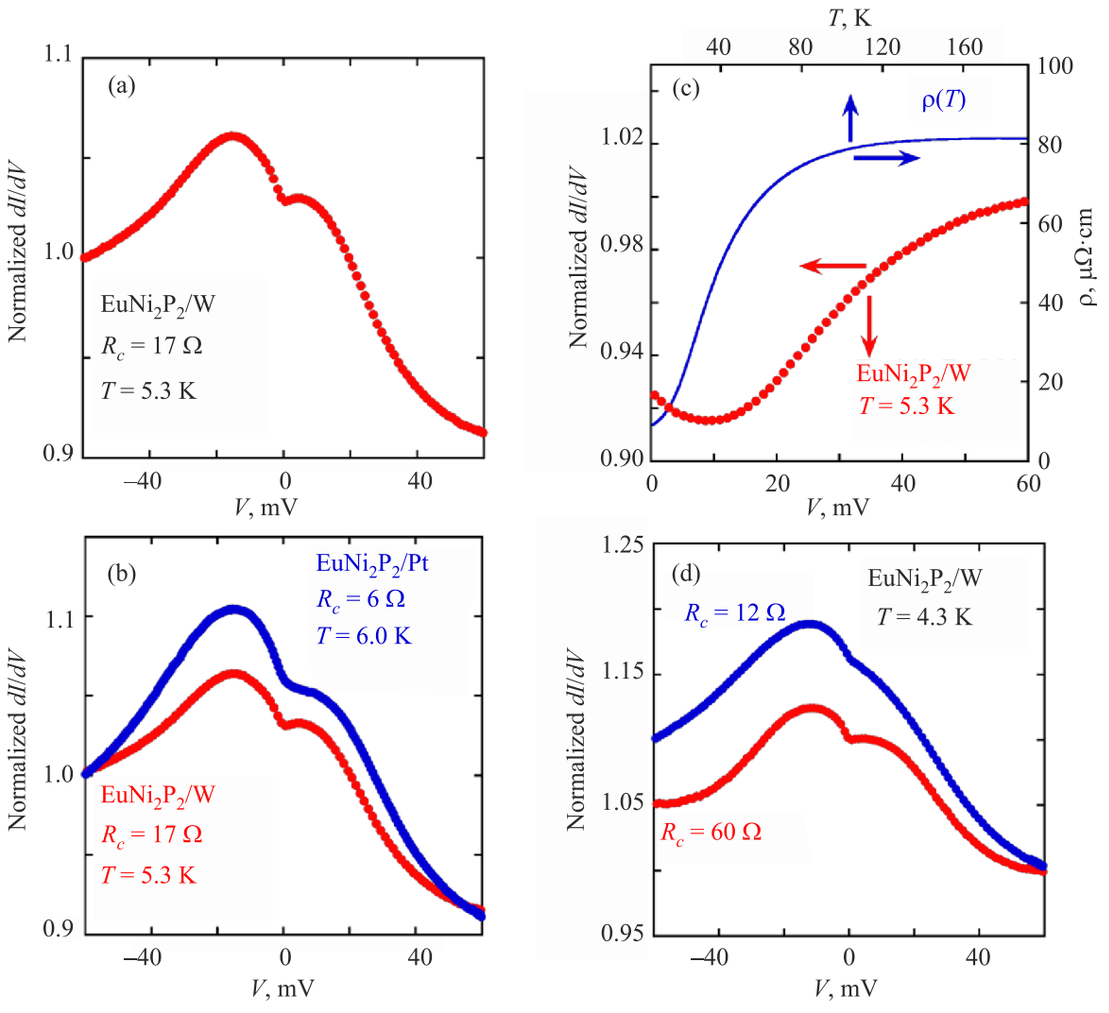

Fig. 1. (Color online) (a) Differential conductance (dI/dV) of $EuNi_2P_2$/W interface at T = 5.3 K, where the contact resistance R_c = 17 Ω. (b) Differential conductance (dI/dV) of $EuNi_2P_2$/W interface at T = 5.3 K and R_c = 17 Ω (red circles). $EuNi_2P_2$/Pt interface at T = 6.0 K and R_c = 6 Ω (blue circles). (c) Temperature dependence of electrical resistivity ρ(T) (blue) and symmetric part of differential resistance dV/dI (red) for the positive bias voltage in the spectrum plotted in (a). The temperature of the horizontal axis for dV/dI curve is estimated from T_J (see text). (d) Contact size dependence of differential conductance (dI/dV) of $EuNi_2P_2$/W interface at T = 4.3 K. The spectra are measured with increasing contact resistance from R_c = 12 to 60 Ω.

Figure 2(a) shows the temperature dependence of the dI/dV spectra between 5.3 and 56 K. With increasing temperature, the double-peak structure shifts to a lower bias side, and then the double-peak structure becomes unclear at 56 K, suggesting that the asymmetric double-peak structure originates from the indirect hybridization gap. Indeed, a similar behavior was observed in PCS investigations of U-based HF compounds [17, 24]. To evaluate the value of the indirect hybridization gap Δ_{hyb}, we analyzed the spectra using the theoretical model proposed by Maltseva, Dzero, and Coleman (MDC model), which estimates the electron tunneling spectra from a probe tip to a Kondo lattice [11]. The differential tunneling conductance G (eV) in Kondo lattice systems is given by

$$G(eV) \propto \left(1+\frac{q\Delta}{eV-\lambda-i\Gamma}\right)^2 \times \ln\left[\frac{eV-i\Gamma+D_1-\frac{\nu^2}{eV-\lambda-i\Gamma}}{eV-i\Gamma-D_2-\frac{\nu^2}{eV-\lambda-i\Gamma}}\right]+\frac{1}{eV-\lambda-i\Gamma}, \quad (2)$$

where Γ, Δ, λ, and ν are the broadening parameter, width of Kondo resonance, renormalized f level, and hybridization amplitude, respectively. q is the Fano parameter, which is defined as the ratio of the amplitude of two tunneling electron paths from a probe tip to conduction band and f band. Moreover, $-D_1$ and D_2 are the lower and the upper con-

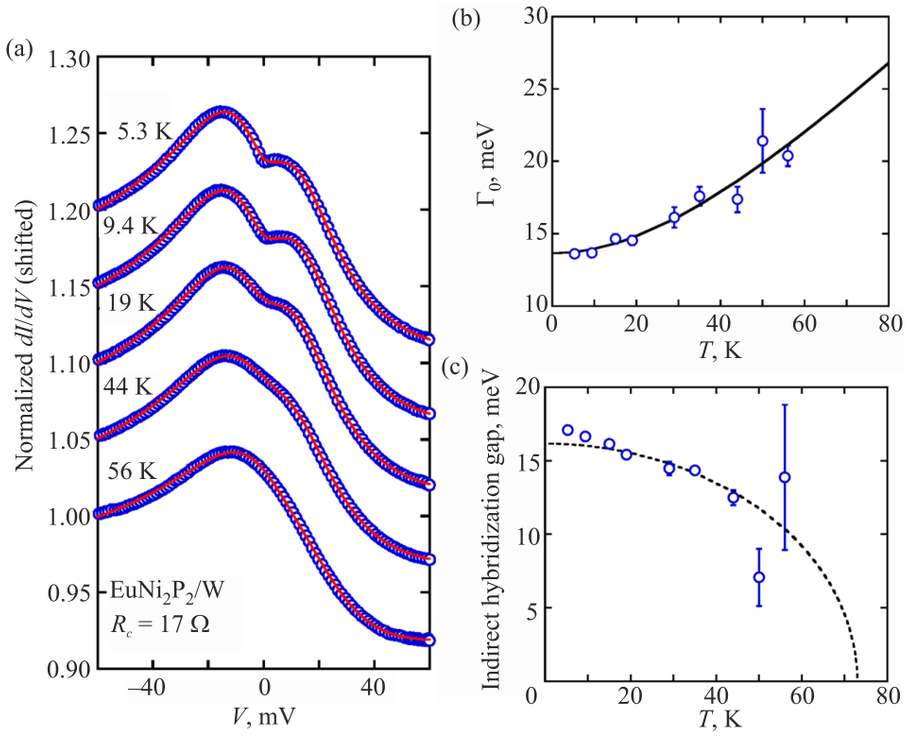

Fig. 2. (Color online) (a) Temperature dependence of differential conductance dI/dV at $EuNi_2P_2$/W interface at R_c = 17 Ω. The solid lines show the theoretical fitting by using MDC model. (b) Temperature dependence of the broadening parameter Γ_0. The solid line represents fitting by Eq. (3), where $\alpha = 3.4 \pm 0.4$. (c) Temperature dependence of the indirect hybridization gap Δ_{hyb} evaluated by the MDC model. The dashed line shows the fitting by Eq. (4). The error bars indicate the 90% confidence interval.

duction band edges, and $2D = D_1+D_2$ is the band width. By fitting the observed PCS spectra using Eq. (2), we estimate the value of indirect hybridization gap, which is given by $\Delta_{hyb} = 2v^2/D$. The details of the analysis are presented in the Supplemental Material in Ref. 26. The PCS spectra are well reproduced by the MDC model as shown in Fig. 2(a), indicating that the asymmetric double-peak structure is caused by the formation of an indirect hybridization gap near the Fermi level in the electronic DOS.

Figure 2(b) illustrates the temperature dependence of the broadening parameter Γ_0, which was evaluated using the MDC model. The localized characteristics of 4*f* electrons can be observed in this parameter. With increasing temperature, Γ_0 increases monotonically and can be fitted by the following equation:

$$\Gamma_0 = \sqrt{(\alpha k_B T)^2 + (2k_B T_K)^2}, \qquad (3)$$

where α is a constant. This formula was utilized to fit the single-site Kondo resonance [39, 40]. The fitting parameter $\alpha = 3.4$ is obtained from the present measurements, consistent with $\alpha = \pi$ for the single-site Kondo model [39, 40]. Notably, Γ_0/k_B extrapolated to $T = 0$ K was estimated to be 79 K, which is in good agreement with the Kondo temperature of $EuNi_2P_2$ obtained by transport measurements [36].

The temperature dependence of the indirect hybridization gap Δ_{hyb} evaluated using the MDC model, is shown in Fig. 2(c). We fitted the temperature dependence of the gap $\Delta_{hyb}(T)$ using the following equation:

$$\Delta_{hyb}(T) = \Delta_0 \sqrt{1 - \left(\frac{T}{T_0}\right)^2}. \qquad (4)$$

Here, Δ_0 is the peak separation at $T = 0$ K and T_0 is the critical temperature at which the indirect hybridization gap appears. Figure 2(c) shows that the gap develops below $T_0 = 73$ K, which is almost the same as the Kondo temperature of $EuNi_2P_2$ [36]. As the temperature increased, the peak separation increased, and $\Delta_{hyb} \sim 16$ meV at $T = 5.3$ K. This value is consistent with that observed in optical conductivity measurements, in which the spectrum exhibits a shoulder-like structure arising from the indirect hybridization gap at approximately 20 meV at $T = 6$ K [41].

As described above, the observed spectroscopic features were well-reproduced by the MDC model, demonstrating that the temperature dependence of the asymmetric double-peak structure reflects the evolution of the indirect hybridization gap developed in $EuNi_2P_2$. In other words, as the temperature decreases, the HF state develops with the formation of an indirect hybridization gap.

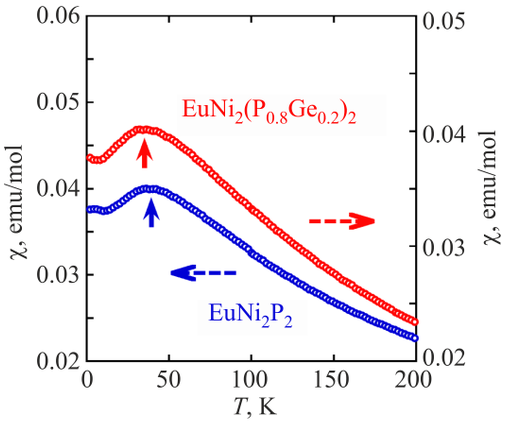

Fig. 3. Temperature dependence of the magnetic susceptibility in $EuNi_2P_2$ and $EuNi_2(P_{0.8}Ge_{0.2})_2$. The external magnetic field $B_{ext} = 0.5$ *T* is applied in parallel with the (001) sample plane. The solid arrows denote the hump position of the spectra, suggesting that the hump position slightly shifts to low temperature by the Ge substitution.

We propose that the origin of the HF in $EuNi_2P_2$ is caused by the valence fluctuation and not by the spin fluctuation from the detailed analysis of the PCS spectra [26]. To examine this scenario, that is, the role of valence fluctuation in the emergence of HF behavior, we performed a PCS investigation in a Ge-substituted $EuNi_2(P_{0.8}Ge_{0.2})_2$. Figure 3 shows the temperature dependence of the magnetic susceptibility in $EuNi_2P_2$ and $EuNi_2(P_{0.8}Ge_{0.2})_2$, in which the external magnetic field B_{ext} = 0.5 T is applied in parallel with the (001) sample plane. The magnetic susceptibility of $EuNi_2P_2$ follows the Curie–Weiss law in the high-temperature region above 150 K. As the temperature decreases below 150 K, the magnetic susceptibility deviates downward from the Curie–Weiss law and then shows a hump structure at $T \sim 40$ K. The temperature dependence of the magnetic susceptibility in $EuNi_2(P_{0.8}Ge_{0.2})_2$ is similar to that in $EuNi_2P_2$, whereas the hump structure in $EuNi_2(P_{0.8}Ge_{0.2})_2$ is observed at $T \sim 35$ K. Namely, the hump structure shifts to lower temperatures by Ge substitution, implying the suppression of the Kondo temperature.

Figure 4(a) plots the *dI*/*dV* spectra on $EuNi_2(P_{0.8}Ge_{0.2})_2$ and $EuNi_2P_2$. The asymmetric double-peak structure is clearly observed in both spectra, while the peak position is slightly shifted to the lower bias side by the Ge substitution. The temperature dependence of the *dI*/*dV* spectra is depicted in Fig. 4(b). As the temperature increases, the double-peak structure shifts to the low bias side, which is blurred at around 36 K. To estimate the indirect hybridization gap Δ_{hyb} in $EuNi_2(P_{0.8}Ge_{0.2})_2$, we analyze the spectra using the MDC model, as shown in Fig. 4(b). The spectra can be reproduced by the MDC model, indicating that the asymmetric double-peak structure originates from the indirect hybridization gap formed in the electronic DOS. Figure 5 shows the temperature dependence of $\Delta_{hyb}(T)$ estimated by using the MDC model. The gap decreases with increasing temperature, similarly to that of $EuNi_2P_2$. We fit the temperature dependence of the gap $\Delta_{hyb}(T)$ by Eq. (4). As illustrated by the solid line in Fig. 5, the equation well-reproduces the experimental results, in which 6 meV and 58 K are used as the fitting parameters

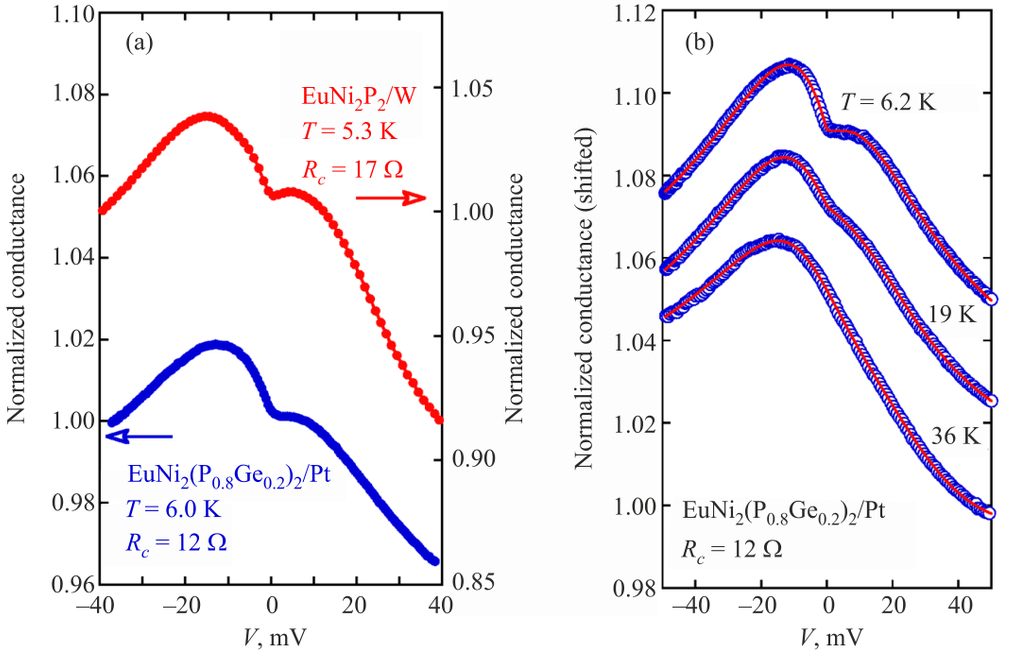

Fig. 4. (Color online) (a) Differential conductance *dI*/*dV* spectrum on $EuNi_2P_2$ (red circles) and $EuNi_2(P_{0.8}Ge_{0.2})_2$ (blue circles) measured with a Pt- and a W-probe tip, respectively. (b) Temperature dependence of the differential conductance *dI*/*dV* spectrum at $EuNi_2(P_{0.8}Ge_{0.2})_2$/Pt interface. The solid lines show the theoretical fitting by using MDC model.

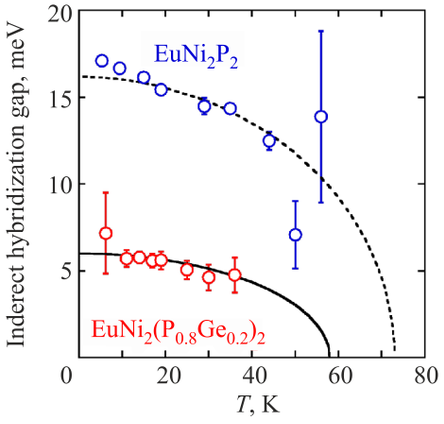

Fig. 5. (Color online) Temperature dependence of the indirect hybridization gap Δ_{hyb} evaluated from the MDC model. The blue and red circles depict the date for $EuNi_2P_2$ and $EuNi_2(P_{0.8}Ge_{0.2})_2$, respectively. The dashed and solid lines are fitting using Eq. (4). The error bars indicate the 90% confidence interval.

for Δ_0 and T_0, respectively. Moreover, in the case of $EuNi_2P_2$, Δ_0, and T_0 are estimated to be 16 meV and 73 K, respectively, as shown as a dashed line in Fig. 5. As mentioned above, T_0 corresponds to the Kondo temperature. Hence, the Kondo temperature decreases by the Ge substitution, which is consistent with the magnetic susceptibility measurements, as shown in Fig. 3. The results demonstrate that the Ge substitution suppresses the Kondo temperature and the indirect hybridization gap $\Delta_{hyb}(T)$.

As described above, the spectroscopic features of the PCS spectra of $EuNi_2(P_{0.8}Ge_{0.2})_2$ are well-explained by the MDC model, similar to those of $EuNi_2P_2$, although $\Delta_{hyb}(T)$ is suppressed. The results indicate that the suppression of the valence fluctuation by Ge substitution reduces the c–f hybridization, decreasing the indirect hybridization gap $\Delta_{hyb}(T)$. Recalling that a large Sommerfeld coefficient is confirmed up to $x = 0.3$ for $EuNi_2(P_{1-x}Ge_x)_2$ in the specific heat [31], the results strongly suggest the emergence of HF behavior in the present system is related to valence fluctuation. Further PCS investigations in samples with high Ge concentrations are indispensable for understanding the origin of HF behavior.

3.2. YbPd

YbPd with a cubic CsCl-type structure is a valence-fluctuating system with an average Yb valence of 2.8+ [42]. As the temperature decreases, the cubic structure transforms to a tetragonal structure at $T_1 = 125$ K. At $T_2 = 105$ K, two-dimensional (2D) layers composed of $Yb^{2.6+}$ and $Yb^{3.0+}$ ions

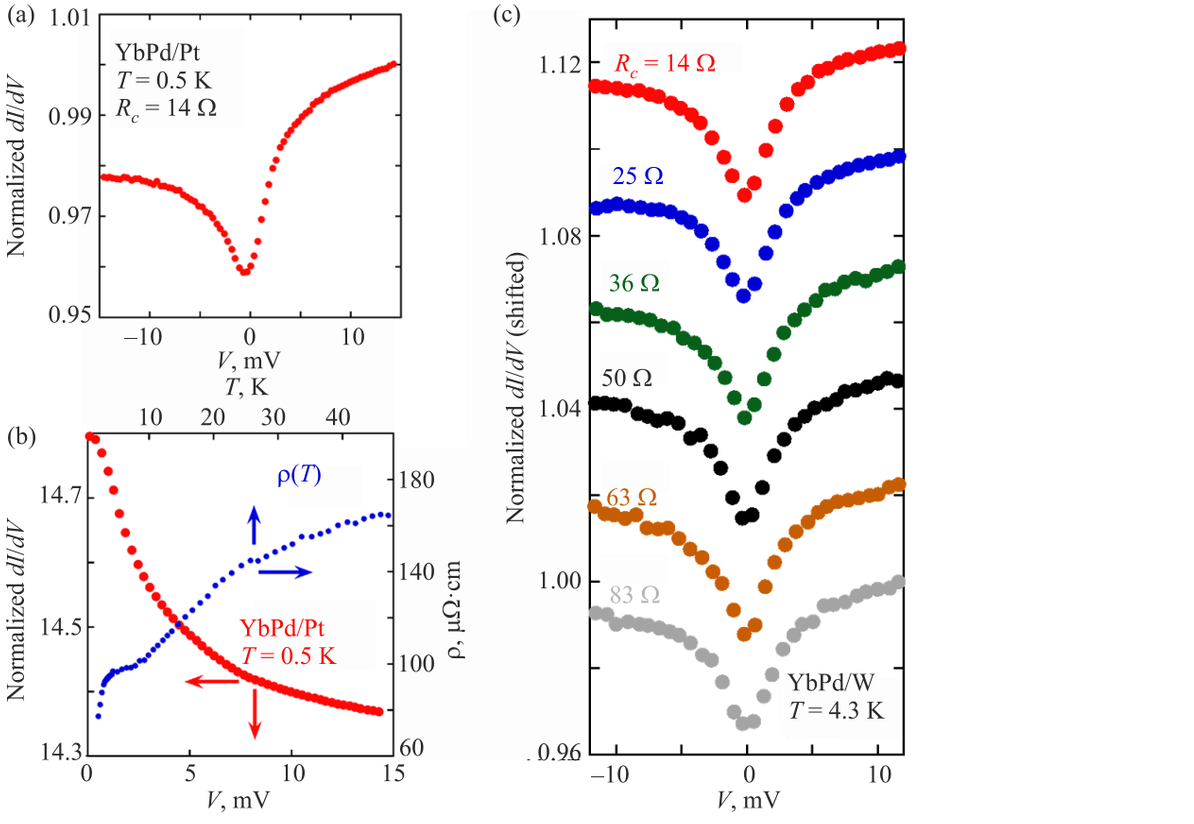

Fig. 6. (Color online) (a) Differential conductance (dI/dV) of Yb/Pt interface at $T = 0.5$ K, where the contact resistance $R_c = 14$ Ω. (b) Temperature dependence of electrical resistivity ρ(T) (blue) and symmetric part of differential resistance dV/dI (red) for the positive bias voltage in the spectrum plotted in (a). The temperature of the horizontal axis for dV/dI curve is estimated from T_J (see text). (c) Contact size dependence of differential conductance (dI/dV) of YbPd/W interface at $T = 4.3$ K. The spectra are measured with increasing contact resistance from $R_c = 14$ to 83 Ω.

are alternately aligned along the *c* axis in the tetragonal structure, as confirmed by resonant X-ray diffraction [43]. This means that valence fluctuating Yb ions still exist in YbPd below T_2. Additionally, magnetic phase transitions were observed at $T_3 = 1.9$ K and $T_4 = 0.5$ K [42]. The transport properties of YbPd differ significantly from those of other valence ordering systems, such as Yb_4As_3 [44, 45], Eu_4As_3 [46], and Eu_3S_4 [47], in which rare earth ions have integer valence values. The temperature dependence of the electrical resistivity $\rho(T)$ of YbPd shows metallic behavior even below T_2, despite the valence ordering. Additionally, neutron diffraction experiments revealed that the magnitude of the magnetic moment of the Yb^{3+} site at low temperature is much smaller than that expected from the Γ_8 crystal-electric-field ground state in addition to the zero moment of the 2.6+ site, implying the emergence of the Kondo effect [48]. The reported Sommerfeld coefficient for specific heat is large [49]. These results suggest the formation of a Kondo lattice below T_2. To reveal the role of the valence fluctuation at $Yb^{2.6+}$ sites in the suppression of magnetic moments of Yb^{3+} sites and the emergence of Kondo behavior in YbPd, we studied the electronic DOS near the Fermi level with PCS measurements on YbPd.

Figure 6(a) shows the differential conductance *dI*/*dV* spectrum of the YbPd/Pt interface at $T = 0.5$ K. The spectrum exhibits a zero-bias dip structure with an asymmetric background. To evaluate the local heating effect near the point contact, we compared the bias voltage dependence of the symmetric component of the differential resistance *dV*/*dI* to the temperature dependence of $\rho(T)$, as shown in Fig. 6(b). As the temperature decreases, $\rho(T)$ decreases monotonically, whereas the *dV*/*dI* spectrum increases monotonically. The two curves are entirely different, indicating that the local heating effect is negligible in the present measurements. In other words, the present PCS spectra contain spectroscopic information for YbPd.

Figure 6(c) depicts the contact resistance dependence of the PCS spectra of the YbPd/W interface at $T = 4.3$ K, which was recorded by increasing the contact resistance, that is, decreasing the contact size. A zero-bias dip structure with an asymmetric background was clearly observed in all spectra, suggesting that the zero-bias dip structure with an asymmetric background is an essential feature in the PCS spectra of YbPd. Additionally, the half-width of the zero-bias dip structure is almost the same for all of the spectra with different contact sizes, meaning that the zero-bias dip

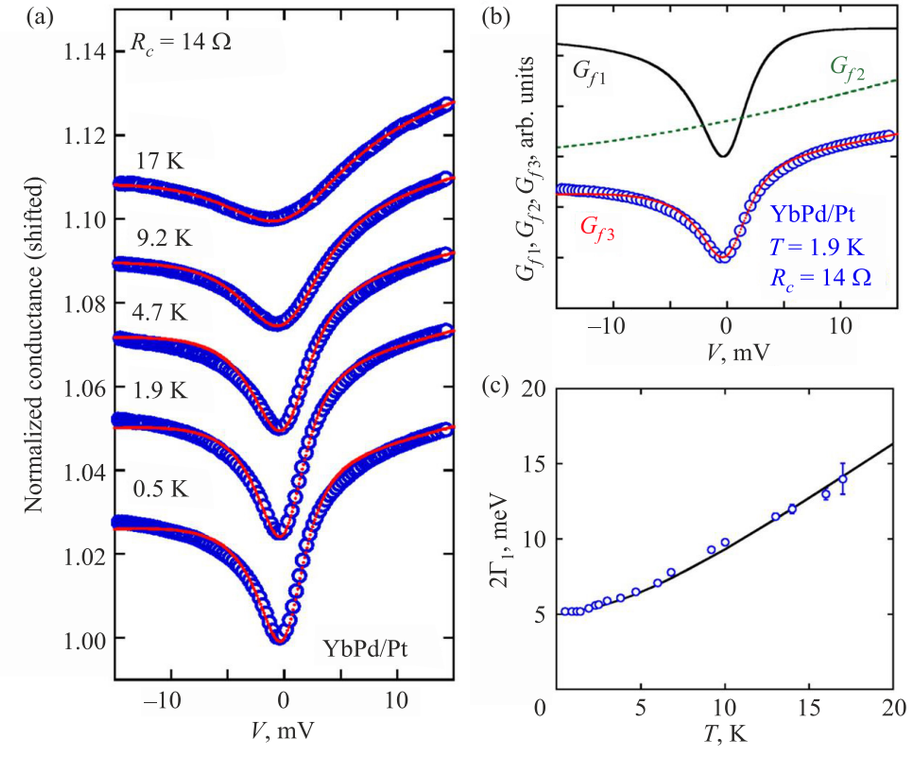

Fig. 7. (Color online) (a) Temperature dependence of differential conductance *dI*/*dV* at YbPd/Pt interface at $R_c = 14$ Ω. The solid lines show the theoretical fitting by two Fano curves [see text and Fig. 7(b)]. (b) Fitting of the spectrum at $T = 1.9$ K by two Fano curves, where $G_{f3} = A_1G_{f1} + A_2G_{f2}$. G_{f1} and G_{f2} are depicted by solid black line and dashed line, while G_{f3} is solid red line. The experimental results of *dI*/*dV* spectra are plotted by circles. The fitting parameters for G_{f1} and G_{f2} are (Γ_1, E_{01}, q_1) = (2.7 meV, 0.15 meV, 0.18), and (Γ_2, E_{02}, q_2) = (70 meV, 5 meV, 0.52). (c) Temperature dependence of the Γ_1 estimated by using two Fano curves as shown in Fig. 7(a). The solid line represents the fitting by Eq. (3). The error bars indicate the 90% confidence interval.

structure does not originate from structural disorder, as in the case of $EuNi_2(P_{1-x}Ge_x)_2$ described in Sec. 3.1. From these results, we conclude that the PCS spectra reflect the intrinsic features of DOS in YbPd.

Figure 7(a) shows the temperature dependence of the dI/dV spectra at R_c = 14 Ω. A zero-bias dip structure with an asymmetric background appears at lower temperatures. As the temperature increases, the dip depth is suppressed, whereas the asymmetric part is unchanged. Moreover, the spectral shape unaffected by the magnetic transition at T_3 = = 1.9 K. The neutron diffraction and specific heat results suggest that the PCS spectra should be discussed based on Kondo resonance, which has been detected in many Kondo systems, such as magnetic impurities adsorbed on a paramagnetic metal [6, 50, 51] and HF systems [23, 25]. The Kondo resonance is reproduced by the Fano model, arising from the interference between the localized electron bands and continuous conduction electron bands. The Fano equation is expressed as follows [52]:

$$G_f(V) \propto \frac{(q+\varepsilon)^2}{1+\varepsilon^2}, \tag{5}$$

where the parameter ε is defined as

$$\varepsilon = \frac{eV - E_0}{\Gamma}. \tag{6}$$

Here, Γ is the half-width at half-maximum (HWHM), E_0 is the center of the resonance, and q is the Fano factor, which represents the ratio of the probabilities between two tunneling paths.

To reproduce the spectra, we suppose that the two Yb sites possess different Kondo temperatures based on previous scanning tunneling spectroscopy experiments [53, 54]. If there are two Kondo resonance states with different Kondo temperatures, the tunneling spectra are reproduced by the summation of the two Fano curves given by Eqs. (5) and (6), respectively. We fitted the PCS spectra of YbPd by summing two Fano curves, $G_{f3} = A_1G_{f1} + A_2G_{f2}$, where G_{f1} is the dip structure, and G_{f2} is the asymmetric background. Figure 7(b) displays the fitting of the PCS spectrum measured at T = 1.9 K, where the fitting parameters for G_{f1} and G_{f2} are (Γ_1, E_{01}, q_1) = (2.7 meV, 0.15 meV, 0.18), and (Γ_2, E_{02}, q_2) = = (70 meV, 5 meV, 0.52), respectively. The spectrum is well-fitted by the summation of the two Fano curves, implying the existence of two Yb sites with different Kondo temperatures.

All the spectra in Fig. 7(a) were successfully reproduced by summing two Fano curves. With increasing temperature, the fitting parameters for G_{f1} are varied, whereas those for G_{f2} are the same as those at T = 0.5 K. A robust valence fluctuation due to the intermediate value of 2.6+ reflects strong c–f hybridization, meaning that the magnetic moment at the $Yb^{2.6+}$ site is fully screened by the conduction electrons. In other words, the Kondo resonance formed at the $Yb^{2.6+}$ site is independent of temperature. Meanwhile, the integer valence value of the Yb^{3+} site represents weak c–f hybridization. Based on these facts, it is reasonable to consider that the asymmetric background spectrum G_{f2} is caused by the Kondo resonance formed at the $Yb^{2.6+}$ site, whereas the zero-bias dip structure G_{f1} originates from that at the Yb^{3+} site.

As described in Sec. 3.1, the temperature dependence of the HWHM for the Kondo resonance is given by Eq. (3). Therefore, in the present case, we substitute $2\Gamma_1$ or $2\Gamma_2$ for Γ_0. The Kondo temperature T_K at the 2.6 + site was estimated to be $\Gamma_2/k_B \sim 800$ K, which is much higher than the experimental temperature. Hence, the parameters for G_{f2} are assumed to be constant. In contrast, Γ_1 increases monotonically with increasing temperature, which is well-reproduced by considering $T_K \sim 30$ K and $\alpha \sim 9$ in Eq. (3), as shown in Fig. 7(c). Figure 8 illustrates the temperature dependence of the dip depth, which increases logarithmically with decreasing temperature and saturates at approximately 1 K. These results also support Kondo resonance as the origin of the zero-bias structure [55, 56].

As presented above, the PCS results demonstrate that Kondo resonance is formed at both sites for Yb^{3+} and $Yb^{2.6+}$ independently, where the Kondo temperatures are ~ 30 and ~ 800 K, respectively. Recalling that the electrical resistivity in YbPd shows metallic behavior even below T_2, it is reasonable to consider that the formation of the Kondo resonance at the $Yb^{2.6+}$ site is responsible for the metallic behavior. However, the zero-bias dip is caused by the Kondo resonance at the magnetic moment of the Yb^{3+} sites screened by conduction electrons, which are provided from the metallic $Yb^{2.6+}$ sites. The observed results strongly suggest that the valence fluctuation at the $Yb^{2.6+}$ site plays a key role in suppressing the magnetic moment of the Yb^{3+} site and the emergence of Kondo lattice behavior in YbPd.

Generally, in HF systems, for example, $EuNi_2P_2$, the PCS spectra show a double-peak structure owing to the for-

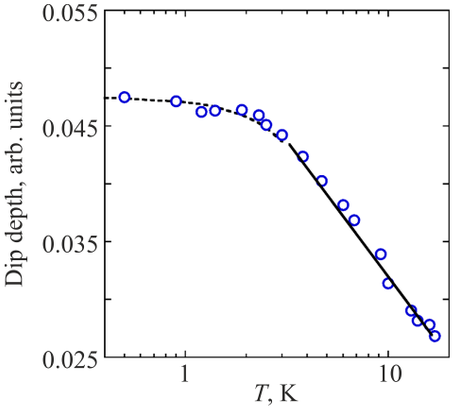

Fig. 8. Temperature dependence of the dip amplitude obtained from Fig. 7(a). The solid and dashed lines show the – ln T dependence and guide for eye, respectively.

mation of an indirect hybridization gap, as discussed in Sec. 3.1. However, the double-peak is invisible in the spectra of YbPd. This is caused by the alternate arrangement of 2D Yb layers with different valence values, preventing 3D HF coherence. Meanwhile, local coherence extends independently in the respective 2D layers. As a result, the two Kondo resonances with different T_K, that is, a single dip structure at zero bias overlapped by an asymmetric background is visible in the spectra. The similar features are reported in the electronic DOS of a van der Waals itinerant magnet Fe_3GeTe_2, which exhibits Kondo lattice behaviors. In the STS and PCS measurements, the spectra are well reproduced by the Fano curve, indicating the emergence of Kondo resonance [57, 58]. From these results, it is reasonable to consider that the extension of 2D coherence suppress the development of indirect hybridization gap.

4. Conclusion

We performed a PCS investigation on a valence-fluctuating Kondo lattice system, $EuNi_2P_2$, and its Ge-substituted system $EuNi_2(Ge_{0.2}P_{0.8})_2$, and YbPd. In $EuNi_2P_2$, the PCS spectra with an asymmetric double-peak structure at approximately zero bias voltage are well-reproduced by the theoretical model of electron tunneling into the Kondo lattice, demonstrating the emergence of an indirect hybridization gap. Moreover, the indirect hybridization gap decreased with increasing Ge substitution. From these results, we conclude that the origin of the HF state in $EuNi_2(P_{1-x}Ge_x)_2$ is related to the valence fluctuation. In YbPd, the PCS spectra exhibit a zero-bias dip structure with an asymmetric background, which can be reproduced by the summation of the two Kondo resonances at the Yb^{3+} and $Yb^{2.6+}$ sites, where the Kondo temperatures are ~ 30 and ~ 800 K, respectively. The observed results strongly suggest that the indirect hybridization gap is detected clearly in Kondo lattice systems with not only strong *c–f* hybridization, but also 3D coherence. On the other hand, the absence of the indirect hybridization gap in the spectroscopic results for several Kondo lattice compounds could be caused by a weak *c–f* hybridization or development of anisotropic coherence. Moreover, we add that PCS is an effective method for examining the evolution of electronic DOS in Kondo lattice systems due to the realization of high tunneling probability of electrons from a probe tip to localized *f* orbital.

Acknowledgment

We thank K. Ienaga for fruitful discussions. We also thank T. Hasuo and K. Yamaguchi for technical support in constructing the ^{3}He cryostat. This work was partially supported by JSPS KAKENHI (Grant No. JP21H01605, JP21H03739, JP23K03304), Nippon Sheet Glass Foundation for Materials Science and Engineering, and Murata Science Foundation.

1. A. C. Hewson, *The Kondo Problem to Heavy Fermions*, Cambridge University Press, Cambridge (1993).
2. H. V. Löhneysen, A. Rosch, M. Vojta, and P. Wölfle, *Rev. Mod. Phys.* **79**, 1015 (2007).
3. Y. Ōnuki, M. Hedo, and F. Honda, *J. Phys. Soc. Jpn.* **89**, 102001 (2020).
4. C. M. Varma, *Rev. Mod. Phys.* **48**, 219 (1976).
5. C. Grenzebach, F. B. Anders, G. Czycholl, and T. Pruschke, *Phys. Rev. B* **74**, 195119 (2006).
6. V. Madhavan, W. Chen, T. Jamneala, M. F. Crommie, and N. S. Wingreen, *Science* **280**, 567 (1998).
7. P. Aynajian, E. H. da Silva Neto, C. V. Parker, Y. Huang, A. Pasupathy, J. Mydosh, and A. Yazdani, *PNAS* **107**, 10 383 (2010).
8. S. Ernst, S. Kirchner, C. Krellner, C. Geibel, G. Zwicknagl, F. Steglich, and S. Wirth, *Nature (London)* **474**, 362 (2011).
9. P. Aynajian, E. H. da Silva Neto, A. Gyenis, R. E. Baumbach, J. D. Thompson, Z. Fisk, E. D. Bauer, and A. Yazdani, *Nature (London)* **486**, 201 (2012).
10. I. Giannakis, J. Leshen, M. Kavai, S. Ran, C.-J. Kang, S. R. Saha, Y. Zhao, Z. Xu, J. W. Lynn, L. Miao, L. A. Wray, G. Kotliar, N. P. Butch, and P. Aynajian, *Sci. Adv.* **5**, eaaw9061 (2019).
11. M. Maltseva, M. Dzero, and P. Coleman, *Phys. Rev. Lett.* **103**, 206402 (2009).
12. Y. G. Naidyuk and I. K. Yanson, *Point-Contact Spectroscopy*, Springer Series in Solid-State Sciences. Springer, New York (2005).
13. W.-C. Lee and L. H. Green, *Rep. Prog. Phys.* **79**, 094502 (2016).
14. P. Szabó, P. Samuely, J. Kačmarčík, T. Klein, J. Marcus, D. Fruchart, S. Miraglia, C. Marcenat, and A. G. M. Jansen, *Phys. Rev. Lett.* **87**, 137005 (2001).
15. M. Tortello, D. Daghero, G. A. Ummarino, V. A. Stepanov, J. Jiang, J. D. Weiss, E. E. Hellstrom, and R. S. Gonnelli, *Phys. Rev. Lett.* **105**, 237002 (2010).
16. M. Shiga, N. Nishimura, Y. Inagaki, T. Kawae, H. Kambara, and K. Tenya, *J. Phys.: Conf. Ser.* **807**, 082001 (2017).
17. W. K. Park, P. H. Tobash, F. Ronning, E. D. Bauer, J. L. Sarrao, J. D. Thompson, and L. H. Greene, *Phys. Rev. Lett.* **108**, 246403 (2012).
18. M. Moser, P. Wachter, J. J. M. Franse, G. P. Meisner, and E. Walker, *J. Magn. Magn. Mater.* **54–57**, 373 (1986).
19. Y. G. Naidyuk, N. N. Gribov, A. A. Lysykh, I. K. Yanson, N. B. Brandt, and V. V. Moshchalkov, *JETP Lett.* **41**, 399 (1985).
20. E. Pauls and G. Voss, *J. Magn. Magn. Mater.* **47–48**, 539 (1985).
21. H. Sato, M. Fujii, K. Yonemitsu, Y. Onuki, and T. Komatsubara, *J. Phys. Soc. Jpn.* **55**, 3295 (1986).
22. Y. G. Naidyuk and I. K. Yanson, *J. Phys.: Condens. Matter* **10**, 8905 (1998).
23. W. K. Park, J. L. Sarrao, J. D. Thompson, and L. H. Greene, *Phys. Rev. Lett.* **100**, 177001 (2008).

24. N. K. Jaggi, O. Mehio, M. Dwyer, L. H. Greene, R. E. Baumbach, P. H. Tobash, E. D. Bauer, J. D. Thompson, and W. K. Park, *Phys. Rev. B* **95**, 165123 (2017).
25. L. Yin, L. Che, T. Le, Y. Zhang, H. Lee, D. Gnida, J. D. Thompson, D. Kaczorowski, and X. Lu, *J. Phys.: Condens. Matter* **33**, 205603 (2021).
26. M. Shiga, I. Maruyama, K. Okimura, H. Takata, T. Takahashi, A. Mitsuda, H. Wada, Y. Inagaki, and T. Kawae, *Phys. Rev. B* **103**, L041113 (2021).
27. M. Shiga, T. Takahashi, T. Teramoto, I. Maruyama, A. Mitsuda, H. Wada, and T. Kawae, *JPS Conf. Proc.* (in press).
28. M. Shiga, K. Okimura, H. Takata, A. Mitsuda, I. Maruyama, H. Wada, Y. Inagaki, and T. Kawae, *Phys. Rev. B* **100**, 245117 (2019).
29. M. Shiga, T. Harada, T. Takahashi, A. Mitsuda, H. Wada, Y. Inagaki, and T. Kawae, *JPS Conf. Proc.* **30**, 011139 (2020).
30. E. V. Sampathkumaran, L. C. Gupta, and R. Vijayaraghavan, *Phys. Lett. A* **88**, 180 (1982).
31. U. B. Paramanik, A. Bar, D. Das, N. Caroca-Canales, R. Prasad, C. Geibel, and Z. Hossain, *J. Phys. Condens. Matter* **28**, 166001 (2016).
32. A. Mitsuda, M. Sugishima, T. Hasegawa, S. Tsutsui, M. Isobe, Y. Ueda, M. Udagawa, and H. Wada, *J. Phys. Soc. Jpn.* **82**, 084712 (2013).
33. M. Shiga, N. Nishimura, H. Takata, Y. Inagaki, H. Kambara, K. Tenya, and T. Kawae, *J. Phys.: Conf. Ser.* **897**, 012001 (2017).
34. R. Nagarajan, G. K. Shenoy, L. C. Gupta, and E. V. Sampathkumaran, *Phys. Rev. B* **32**, 2846 (1985).
35. R. A. Fisher, P. Radhakrishna, N. E. Phillips, J. V. Badding, and A. M. Stacy, *Phys. Rev. B* **52**, 13519 (1995).
36. Y. Hiranaka, A. Nakamura, M. Hedo, T. Takeuchi, A. Mori, Y. Hirose, K. Mitsumura, K. Sugiyama, M. Hagiwara, T. Nakama, and Y. Onuki, *J. Phys. Soc. Jpn.* **82**, 083708 (2013).
37. D. C. Ralph, A. W. W. Ludwig, J. von Delft, and R. A. Buhrman, *Phys. Rev. Lett.* **72**, 1064 (1994).
38. R. J. P. Keijsers, O. I. Shklyarevskii, and H. van Kempen, *Phys. Rev. B* **51**, 5628 (1995).
39. T. A. Costi, A. C. Hewson, and V. Zlatic, *J. Phys. Condens. Matter* **6**, 2519 (1994).
40. K. Nagaoka, T. Jamneala, M. Grobis, and M. F. Crommie, *Phys. Rev. Lett.* **88**, 077205 (2002).
41. V. Guritanu, S. Seiro, J. Sichelschmidt, N. Caroca-Canales, T. Iizuka, S. Kimura, C. Geibel, and F. Steglich, *Phys. Rev. Lett.* **109**, 247207 (2012).
42. R. Pott, W. Boksch, G. Leson, B. Politt, H. Schmidt, A. Freimuth, K. Keulerz, J. Langen, G. Neumann, F. Oster, J. Röhler, U. Walter, P. Weidner, and D. Wohlleben, *Phys. Rev. Lett.* **54**, 481 (1985).
43. R. Takahashi, T. Honda, A. Miyake, T. Kagayama, K. Shimizu, T. Ebihara, T. Kimura, and Y. Wakabayashi, *Phys. Rev. B* **88**, 054109 (2013).
44. A. Ochiai, T. Suzuki, and T. Kasuya, *J. Phys. Soc. Jpn.* **59**, 4129 (1990).
45. U. Staub, M. Shi, C. Schulze-Briese, B. D. Patterson, F. Fauth, E. Dooryhee, L. Soderholm, J. O. Cross, D. Mannix, and A. Ochiai, *Phys. Rev. B* **71**, 075115 (2005).
46. A. Ochiai, Y. Shima, and M. Shirakawa, *J. Phys. Soc. Jpn.* **72**, 3174 (2003).
47. R. Pott, G. Güntherodt, W. Wichelhaus, M. Ohl, and H. Bach, *Phys. Rev. B* **27**, 359 (1983).
48. K. Oyama, M. Sugishima, K. Tanabe, A. Mitsuda, H. Wada, K. Ohoyama, T. Matsukawa, Y. Yoshida, A. Hoshikawa, T. Ishigaki, and K. Iwasa, *J. Phys. Soc. Jpn.* **87**, 114705 (2018).
49. Y. Tokiwa, S. Grüheit, H. S. Jeevan, C. Stingl, and P. Gegenwart, *J. Phys.: Conf. Ser.* **273**, 012062 (2011).
50. M. Ternes, A. J. Heinrich, and W.-D. Schneider, *J. Phys.: Condens. Matter* **21**, 053001 (2009).
51. A. R. Schmidt, M. H. Hamidian, P. Wahl, F. Meier, A. V. Balatsky, J. D. Garrett, T. J. Williams, G. M. Luke, and J. C. Davis, *Nature (London)* **465**, 570 (2010).
52. U. Fano, *Phys. Rev.* **124**, 1866 (1961).
53. E. Minamitani, N. Tsukahara, D. Matsunaka, Y. Kim, N. Takagi, and M. Kawai, *Phys. Rev. Lett.* **109**, 086602 (2012).
54. K. J. Franke, G. Schulze, and J. I. Pascual, *Science* **332**, 940 (2011).
55. S. M. Cronenwett, T. H. Oosterkamp, and L. P. Kouwenhoven, *Science* **281**, 540 (1998).
56. P. Nozières, *J. Low Temp. Phys.* **17**, 31 (1974).
57. Y. Zhang, H. Lu, X. Zhu, S. Tan, W. Feng, Q. Liu, W. Zhang, Q. Chen, Y. Liu, X. Luo, D. Xie, L. Luo, Z. Zhang, and X. Lai, *Sci. Adv.* **4**, eaao6791 (2018).
58. Deepti Rana, Aswini R, Basavaraja G, Chandan Patra, Sandeep Howlader, Rajeswari Roy Chowdhury, Mukul Kabir, Ravi P. Singh, and Goutam Sheet, *Phys. Rev. B* **106**, 085120 (2022).

Густина електронних станів у валентно-флуктуаційних ґраткових системах Кондо, яка досліджена методом мікроконтактної спектроскопії
(Огляд)

Masanobu Shiga, Isao Maruyama, Akihiro Mitsuda, Hirofumi Wada, Tatsuya Kawae

Розглянуто наше нещодавнє дослідження методом мікроконтактної спектроскопії (PCS) валентно-флуктуаційних ґраткових систем Кондо: $EuNi_2P_2$, Ge-заміщених $EuNi_2(P_{0.8}Ge_{0.2})_2$ та YbPd. Важкоферміонна (HF) сполука $EuNi_2P_2$ демонструє значну флуктуацію валентності через проміжну валентність $Eu^{2,5+}$ при низьких температурах, що призводить до сильної гібридизації між електронами провідності та *f* електронами (*c*–*f* гібридизація). Вимірювання густини електронних станів $EuNi_2P_2$ за допомогою техніки PCS показують, що поведінка HF виникає внаслідок утворення непрямої гібридизаційної щілини з двопіковою структурою поблизу рівня Фермі внаслідок *c*–*f* гібридизації. У $EuNi_2(P_{0.8}Ge_{0.2})_2$ флуктуації ва-

лентності пригнічуються заміщенням Ge, і розділення двопікової структури зменшується. Це свідчить про те, що поведінка HF зумовлена флуктуацією валентності. У YbPd, де двовимірні (2D) шари Yb^{3+} та $Yb^{2.6+}$ розташовані по черзі, HF подібна поведінка з великим коефіцієнтом Зоммерфельда з'являється при низьких температурах у питомій теплоємності. Спектри PCS за структурою являють собою провал при нульовому зміщенні на асиметричному фоні, що відтворюється сумою двох кривих Фано з різними характерними температурами, та означає утворення двох резонансних станів Кондо для Yb^{3+} та $Yb^{2.6+}$. Це свідчить про те, що локальна когерентність зумовлює великий коефіцієнт Зоммерфельда у 2D шарах Yb^{3+}, які екрануються електронами провідності, створеними валентними флуктуаційними ділянками $Yb^{2.6+}$. Одержані результати свідчать про те, що PCS є потужною методикою для дослідження варіації густини електронних станів у валентно-флуктуаційних ґраткових системах Кондо.

Ключові слова: мікроконтактна спектроскопія, густина електронних станів, ґратка Кондо, важкий ферміон, валентна флуктуація.